

Molecular Imaging of Matrix Metalloproteinase Expression in Atherosclerotic Plaques of Mice Deficient in Apolipoprotein E or Low-Density-Lipoprotein Receptor

Satoru Ohshima¹, Artiom Petrov¹, Shinichiro Fujimoto¹, Jun Zhou¹, Michael Azure², D. Scott Edwards²,
Toyoaki Murohara³, Navneet Narula¹, Sotirios Tsimikas⁴, and Jagat Narula¹

¹Division of Cardiology, University of California, Irvine School of Medicine, Irvine, California; ²Lantheus Medical Imaging, North Billerica, Massachusetts; ³Department of Cardiology, Nagoya University Graduate School of Medicine, Nagoya, Japan; and ⁴Division of Cardiovascular Diseases, Department of Medicine, University of California, San Diego School of Medicine, La Jolla, California

Matrix metalloproteinases (MMPs) are expressed in atherosclerotic plaques and play an important role in plaque instability.

Methods: Using ^{99m}Tc-labeled broad-spectrum MMP inhibitor (MPI), we performed noninvasive imaging of MMP expression with micro-SPECT/micro-CT in mice deficient in apolipoprotein E (ApoE^{-/-}, *n* = 14), mice deficient in low-density-lipoprotein receptor (LDLR^{-/-}, *n* = 14), and C57/BL6 mice as controls (*n* = 7). Seven ApoE^{-/-} and 7 LDLR^{-/-} received a high-cholesterol diet. After *in vivo* imaging, aortas were explanted, *ex vivo* images acquired, and the percent injected dose of MPI per gram (%ID/g) determined, followed by histologic characterization of atherosclerotic lesions. **Results:** MPI uptake was noninvasively visualized in atherosclerotic lesions by micro-SPECT, with confirmation by micro-CT of anatomic location and aortic calcification. %ID/g in each part of the aorta was highest in ApoE^{-/-} that were fed a high-cholesterol diet, followed by LDLR^{-/-} that were fed a high-cholesterol diet, ApoE^{-/-} that were fed normal chow, and LDLR^{-/-} that were fed normal chow. The control mice had minimal MPI uptake. A significant correlation was noted between %ID/g and % area positive for macrophages (*r* = 0.81, *P* = 0.009), MMP-2 (*r* = 0.65, *P* = 0.013), and MMP-9 (*r* = 0.62, *P* = 0.008).

Conclusion: This study demonstrates the usefulness of molecular imaging for noninvasive assessment of the extent of MMP expression in various transgenic mouse models of atherosclerosis receiving a normal or hyperlipidemic diet. It is conceivable that such a strategy may be translationally developed for identification of unstable atherosclerotic plaques.

Key Words: radionuclide imaging; atherosclerosis; plaque rupture; apolipoprotein E-deficient mice; low-density-lipoprotein receptor-deficient mice

J Nucl Med 2009; 50:612–617

DOI: 10.2967/jnumed.108.055889

Received Jul. 14, 2008; revision accepted Dec. 29, 2008.

For correspondence or reprints contact: Artiom Petrov, C116, Medical Science I, UC-Irvine Main Campus, Irvine, CA 92697.

E-mail: adpetrov@uci.edu

COPYRIGHT © 2009 by the Society of Nuclear Medicine, Inc.

Accumulation of inflammatory cells and release of cytokines in vascular subintima contribute to initiation, maturation, and instability of atherosclerotic lesions (1–3). Production of matrix metalloproteinases (MMP) in inflamed plaques has been proposed to mediate expansive vascular remodeling after the breakdown of extracellular matrix (1,4,5). Increased MMP expression and activity in the plaque may also result in gradual dissolution of matricial content in the fibrous cap and further render the atheromatous lesion unstable. It is therefore reasonable to assume that development of noninvasive strategies to determine MMP activity in atherosclerotic plaques would allow one to assess the extent of vascular instability, define appropriate management, and evaluate the efficacy of therapeutic interventions. Recently, 2 approaches have been described for the *in vivo* assessment of MMP activity in atherosclerotic lesions (4–8). The first approach uses an MMP substrate that can be activated and is linked to an appropriate detection tracer that is cleaved only in lesions expressing active MMP; the targeting probe is then trapped intracellularly for imaging (6). The other approach uses radiolabeled broad-spectrum inhibitors of active MMP; the tracer binds only to the lesions that demonstrate significant MMP activity (4,5,7,8).

Mice deficient in apolipoprotein E (ApoE^{-/-}) and mice deficient in low-density-lipoprotein receptor (LDLR^{-/-}) exhibit spontaneous hyperlipidemia and the development of extensive atherosclerosis in the aorta and large arteries (9–11). More extensive hyperlipidemia and lesions develop in ApoE^{-/-}, particularly when fed a high cholesterol diet, than in LDLR^{-/-} (10). The lesion morphology in these mice is similar to that of human atherosclerosis (10–13). In the present study, we used a ^{99m}Tc-labeled broad MMP

inhibitor (MPI) to evaluate the feasibility of noninvasive imaging of variable expression of MMP activity in atherosclerotic lesions in these 2 transgenic mouse models, which received either normal chow or a high-cholesterol diet. Because MMP activity in atherosclerotic lesions is considered to be associated with plaque instability, we proposed that noninvasive assessment of MMP activity would allow identification of lesions that are susceptible to plaque rupture and acute coronary events. Two different transgenic mouse models and 2 different diet regimens were used to develop a spectrum of atherosclerotic lesion severities, and hence variable MMP activity, so that the usefulness of a molecular imaging strategy to determine the extent of MMP expression could be established.

MATERIALS AND METHODS

Classification of Animals

The mice used in this study were obtained from the Jackson Laboratory. The 35 mice were 62 ± 3.3 (mean \pm SD) wk old. There were 14 homozygous ApoE^{-/-} (hybrid with a C57/BL6 \times 129 ola background), 14 homozygous LDLR^{-/-} (with a C57/BL6 \times 129 Sv background), and, as disease controls, 7 wild-type mice with the same genetic background (C57/BL6). Of 14 ApoE^{-/-} and 14 LDLR^{-/-}, 7 in each group received normal mouse chow and were fed a diet containing 0.15% cholesterol for 12 mo before imaging. The 2 transgenic mouse models demonstrate significantly different severities and locations of atherosclerotic disease. Further, use of a hypercholesterolemic, or Western, diet exaggerates the atherosclerotic disease. The wild-type mice were aged for the same length of time and in the same environment as the transgenic mice and were used as negative controls for the imaging study. The study protocol for imaging and tissue harvesting conformed to the guidelines for the care and use of laboratory animals established by the National Institutes of Health (NIH publication 85-23, revised 1996) and was approved by the Institutional Laboratory Animal Care and Use Committee at the University of California, Irvine.

Targeting Probe and Radiolabeling

The targeting probe, MPI, comprises a broad-spectrum MMP-inhibiting macrocyclic compound (RP805; Lantheus Medical Imaging Inc.), which was radiolabeled with ^{99m}Tc. The structure of MPI has been reported previously (8). This compound binds to the exposed catalytic domain of MMPs. Our previous *in vitro* and *in vivo* blocking experiments have demonstrated the specificity of radiotracer for metalloproteinase activity (5).

For radiolabeling, the contents of a vehicle vial were dissolved in 0.5 mL of 0.9% sterile saline, and the clear solution was transferred to a vial containing 25–35 μ g of MPI precursor. The mixture was incubated for 10 min to ensure dissolution of all particles, and an aliquot of ^{99m}Tc-pertechnetate eluate (1.0 mL, \sim 3,330 MBq/mL) was added. The reaction vial was heated at 100°C for 10 min, followed by high-pressure liquid chromatography; the radiolabeling efficiency was more than 97%. Each mouse was injected with 0.10 ± 0.01 mL of ^{99m}Tc-MPI (206.5 \pm 19.6 MBq) through the dorsal tail vein.

In Vivo and Ex Vivo Imaging Protocols

The animals were anesthetized with 2.0% isoflurane for imaging. Radionuclide imaging was performed 3 h after radiotracer administration using a dual-head micro-SPECT γ -camera equip-

ped with micro-CT (X-SPECT; γ -Medica, Inc.). SPECT images of the aorta were acquired in 32 steps (120 s per step) at the 140-keV photopeak of ^{99m}Tc with 15% windows using a low-energy, high-resolution pinhole collimator; (aperture size, 1 mm; field of view, 12.5 \times 0.5 cm); the images were acquired in 64 \times 64 matrix format. Immediately after SPECT, a micro-CT scan was obtained without moving the animal. The micro-CT component, comprising an x-ray tube operating at 50 kVp and 0.6 mA, captured 256 views (2.5 s/view) in a 360° rotation. The micro-CT and micro-SPECT images were fused, allowing scintigraphic and anatomic information to be combined in all tomographic scans in 3 different spatial axes. After the *in vivo* imaging, the animals were sacrificed, and the aortas were carefully harvested after perfusion and fixation. The *ex vivo* planar image of the aorta was acquired for 30 min in a 128 \times 128 matrix using a low-energy, high-resolution, parallel-hole collimator (10 holes; diameter, 1.2 mm).

Aorta Harvest and Tissue Preparation

Blood was collected by cardiac puncture at the time of sacrifice, and the animals were perfused and fixed through the same left ventricular puncture under physiologic pressure with cold phosphate-buffered saline followed by 4% paraformaldehyde in phosphate-buffered saline (pH 7.4). After perfusion, the entire aorta was exposed and removed with the surrounding fat and connective tissue. After cleaning the aorta, *ex vivo* images were obtained (as described above). Thereafter, each aorta was divided in arch, thoracic, and abdominal segments for γ -counting. The tissue samples were fixed overnight with 4% paraformaldehyde at 4°C and stored in phosphate-buffered saline with 0.02% sodium azide (NaN₃) at 4°C until further processing.

Quantitative MPI Uptake in Atherosclerosis and Radiotracer Biodistribution

For quantitative estimates of radiotracer uptake, 3 aortic segments were weighed and γ -counted in an automatic well-type γ -counter (Perkin Elmer Wallac Inc.) for calculation of the percent injected dose of MPI per gram (%ID/g) in aortic tissue. In addition, biodistribution studies for the blood, heart, lung, spleen, and kidney were also performed, and the uptake in each tissue was expressed as %ID/g. To correct for radioactive decay and to permit calculation of the concentration of radioactivity as a fraction of the administered dose, aliquots of the injected dose were set aside and counted with the aortic segments and organs.

Histologic and Immunohistochemical Characterization of Aortic Segments

Each aortic segment was further subdivided into 2 equidistant sections and packed in a normal rabbit aorta followed by end-on embedding. Packing 5–6 aortic segments together allows flawless cross-sectioning of the aorta in paraffin. Serial 5- μ m-thick sections were cut and mounted on slides pretreated with Vectabond reagent (SP-1800; Vector). Removal of the paraffin was followed by dehydration (\times 2) and staining with Movat pentachrome stain. Histologic specimens were analyzed using the American Heart Association classification (14).

Before immunohistochemical staining, which was performed using a standard method (5) on tissue sections that had been freed of paraffin, endogenous peroxidase and nonspecific background staining were blocked. Macrophages were detected with Mac-3 antibody (0.16 μ g/mL, 550292; BD Biosciences), and smooth muscle cells were stained with antiactin antibody (0.25 μ g/mL, SMA, MAB1420; R&D). Sections were incubated with the primary

antibody overnight at 4°C, followed by biotinylated secondary antibody. Thereafter, ABC kit reagent (Vector) and diaminobenzidine (Vector) were used for color reaction. For immunohistochemical MMP staining, rabbit poly-antibody 37150 (1 µg/µL, MGPLLATFWPEK; Abcam) for MMP-2 and rabbit poly-antibody 16306 (1 µg/µL, intravenous, ab-3; Abcam) for MMP-9 were used. After antigen retrieval with Antigen Unmasking Solution H-3300 (Vector) at 90°C, the sections were incubated overnight at 4°C with primary antibody followed by antirabbit secondary antibody, and color reaction was developed with an ABC kit reagent and diaminobenzidine as reported earlier (5). Histologic and immunohistochemical staining were observed under an Axiovert-200 inverted microscope (Carl Zeiss), and images were acquired with a AxioCam high-resolution digital color camera (1,300 × 1,030 pixels; Carl Zeiss) using Axiovision 3.1 software (Carl Zeiss). Five to 8 images were obtained for each mouse and were analyzed using the KS300 program (Carl Zeiss). The percentage positive immunostained area (immunostained area/total intimal area × 100) was determined for all markers and was evaluated by averaging the percentage positive area of several images per section that covered most to all regions of study. All quantitative comparisons for a given marker were performed on each section stained per group simultaneously.

Statistical Analysis

All results are presented as mean ± SD. To determine the statistical significance of differences between groups, 1-way ANOVA was used, followed by post hoc (Scheffé) analysis for individual group significance. A *P* value of less than 0.05 was considered statistically significant. The correlation between the radiolabeled MPI uptake and the histologic characteristics was evaluated by linear regression analysis.

RESULTS

Noninvasive Imaging of MMP Expression

The atherosclerotic lesions in transgenic mice were clearly visualized by in vivo micro-SPECT using ^{99m}Tc-MPI as the targeting agent. Distribution of the uptake observed on in vivo images was confirmed on ex vivo images of the explanted aorta. Tracer was taken up predominantly in the aortic arch and abdominal aorta of transgenic mice (Fig. 1). No MPI uptake was observed in the control mice. Uptake was significantly more intense in the high-cholesterol-fed transgenic mice than in the normal-chow-fed mice (Fig. 1). On micro-CT images, calcification in the aortic arch was commonly observed; calcification was seen in all high-cholesterol-fed ApoE^{-/-}, in 5 of 7 (71%) normal-chow-fed ApoE^{-/-}, and in 3 of 7 (41%) high-cholesterol-fed

LDLR^{-/-} (Fig. 1). No evidence of calcification was seen in the CT reconstructions of wild-type mice or of LDLR^{-/-} that were fed normal chow. Vertebral anatomy seen on micro-CT images helped identify localization of radiotracer uptake.

Quantitative Estimate of Metalloproteinase Expression

As expected from the in vivo (Fig. 1) and ex vivo images (Fig. 2A) of the aorta, the quantitative MPI uptake (expressed as %ID/g) in each part of aorta (Fig. 2B) was highest in high-cholesterol-fed ApoE^{-/-}, followed by high-cholesterol-fed LDLR^{-/-}, normal-chow-fed ApoE^{-/-}, and normal-chow-fed LDLR^{-/-}. MPI uptake in the thoracic and abdominal aortas was higher in high-cholesterol-fed ApoE^{-/-} than in normal-chow-fed ApoE^{-/-} (thoracic: 0.77% ± 0.24% vs. 0.52% ± 0.12%, *P* = 0.009; abdominal: 0.64% ± 0.31% vs. 0.40% ± 0.14%; *P* = 0.04). However, MPI uptake only in the aortic arch was higher in high-cholesterol-fed LDLR^{-/-} than in normal-chow-fed LDLR^{-/-} (0.81% ± 0.40% vs. 0.48% ± 0.15%, *P* = 0.015). Minimal background activity was observed in the control mice (arch: 0.19% ± 0.05%; thoracic: 0.19% ± 0.07%; abdominal: 0.15% ± 0.04%). MPI uptake was comparable in high-cholesterol-fed transgenic mice of either type (Fig. 2B).

The highest MPI activity in nontargeted organs was in the kidney (25.7% ± 14.6%), followed by liver (0.50% ± 0.14%), spleen (0.44% ± 0.14%), lung (0.34% ± 0.22%), and heart (0.26% ± 0.11%). The blood level of MPI was 0.34% ± 0.10%. The lesion-to-blood ratio in control mice (0.66 ± 0.13) was less than 1.0. In contrast, the ratio in normal-chow-fed ApoE^{-/-}, high-cholesterol-fed ApoE^{-/-}, normal-chow-fed LDLR^{-/-}, and high-cholesterol-fed LDLR^{-/-} was always higher than 1.0 (1.29 ± 0.45, 1.30 ± 0.62, 1.46 ± 0.25, and 1.83 ± 0.19, respectively). No significant differences were observed among blood clearance in the various transgenic mouse groups regardless of cholesterol feeding.

Pathologic Characterization of Atherosclerotic Lesions

The atherosclerotic lesions were seen predominantly in the aortic arch and large vessels and in the abdominal aorta. The lesions were pathologically more advanced in the high-cholesterol-fed ApoE^{-/-}, the normal-chow-fed ApoE^{-/-}, and the high-cholesterol-fed LDLR^{-/-} (Fig. 3). The normal-chow-fed LDLR^{-/-}, the high-cholesterol-fed LDLR^{-/-}, the normal-chow-fed ApoE^{-/-}, and the high-cholesterol-fed ApoE^{-/-} exhibited American Heart Association types I–II,

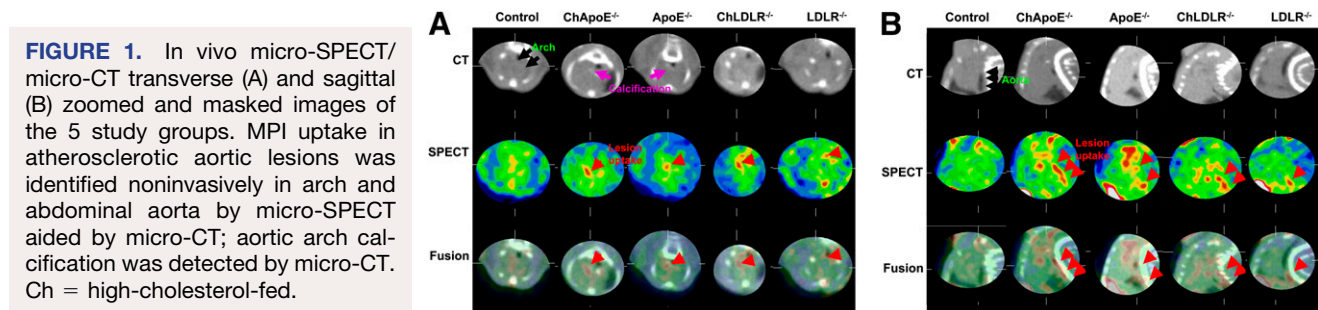


FIGURE 1. In vivo micro-SPECT/micro-CT transverse (A) and sagittal (B) zoomed and masked images of the 5 study groups. MPI uptake in atherosclerotic aortic lesions was identified noninvasively in arch and abdominal aorta by micro-SPECT aided by micro-CT; aortic arch calcification was detected by micro-CT. Ch = high-cholesterol-fed.

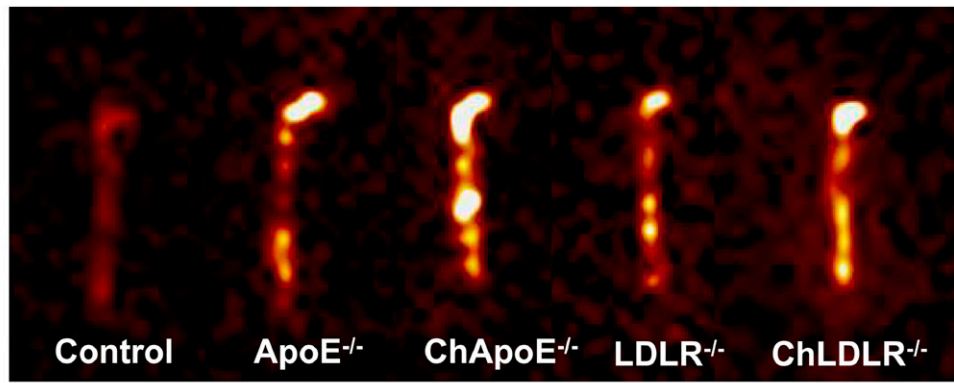
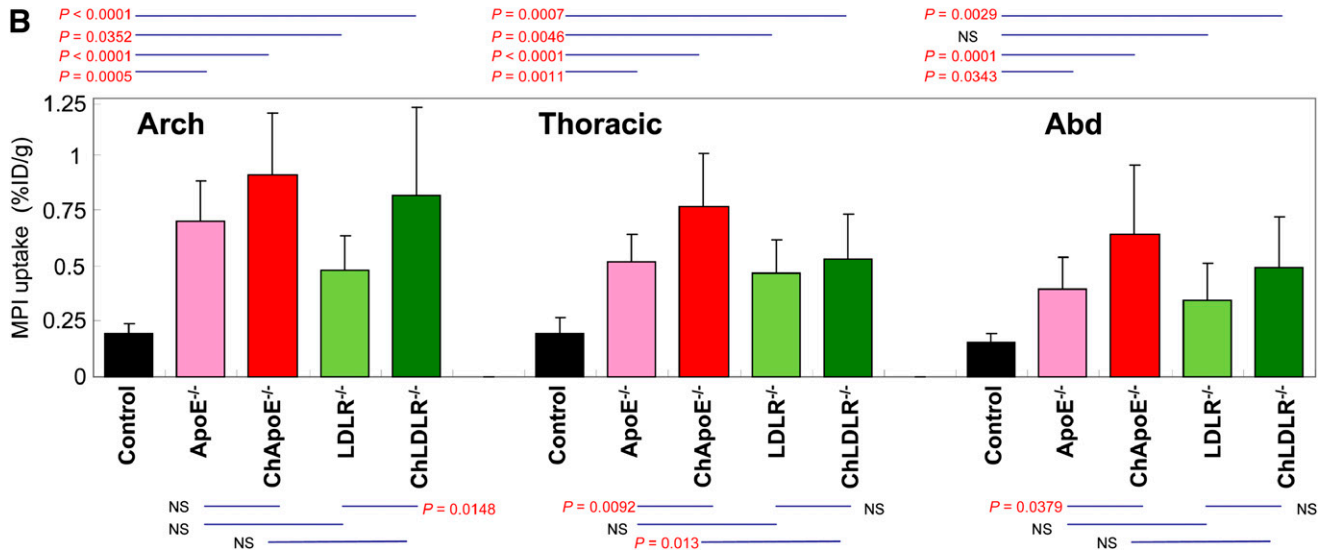
A**B**

FIGURE 2. MPI uptake in aorta by ex vivo imaging (A) and quantitative estimates of tracer uptake (B) in the 5 study groups. Ex vivo imaging reveals background activity in wild-type mice. Uptake in transgenic mice is further enhanced by high-cholesterol diet (Ch). Uptake is most prominently seen in aortic arch. Bar graphs show quantitative ^{99m}Tc-MPI uptake, represented as mean (\pm SD) %ID/g, in each part of aorta in the various animal groups. MPI uptake in B corresponds to ex vivo images in A.

types II–V, type V, and type V lesions, respectively. MPI uptake was increased in proportion to American Heart Association lesion type (0: $0.19\% \pm 0.01\%$; I–II: $0.56\% \pm 0.11\%$; III–IV: $0.75\% \pm 0.04\%$; V: $1.02\% \pm 0.29\%$; $P < 0.0001$).

In the immunohistochemical study, macrophage concentration and MMP-2 and MMP-9 expression were highest in

atherosclerotic lesions in high-cholesterol-fed ApoE^{-/-}, followed by normal-chow-fed ApoE^{-/-}, high-cholesterol-fed LDLR^{-/-}, and normal-chow-fed LDLR^{-/-} (Fig. 4). Although distinctly higher MMP-2 and MMP-9 expression was immunohistologically observed in high-cholesterol-fed ApoE^{-/-} than in high-cholesterol-fed LDLR^{-/-}, this difference was not reflected in %ID/g in the aortic arch and

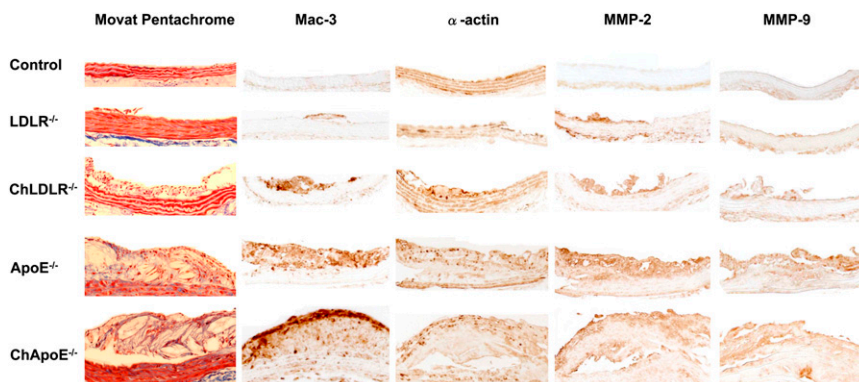


FIGURE 3. Histopathologic and immunohistochemical characterization of atherosclerotic lesions in the 5 study groups. Magnification is $\times 20$. Ch = high-cholesterol-fed.

abdominal aorta. This discrepancy can, at least in part, be explained by the size of the aortic sample. Although %ID/g is generally calculated for 1-cm large aortic specimens, the pathologic section is 5 μ m thick. Regression analysis demonstrated a significant correlation between radiolabeled MPI uptake and macrophage infiltration ($r = 0.81$, $P = 0.009$), as well as between radiolabeled MPI uptake and the expression of MMP-2 ($r = 0.65$, $P = 0.013$) and MMP-9 ($r = 0.62$, $P = 0.008$) (Fig. 4).

DISCUSSION

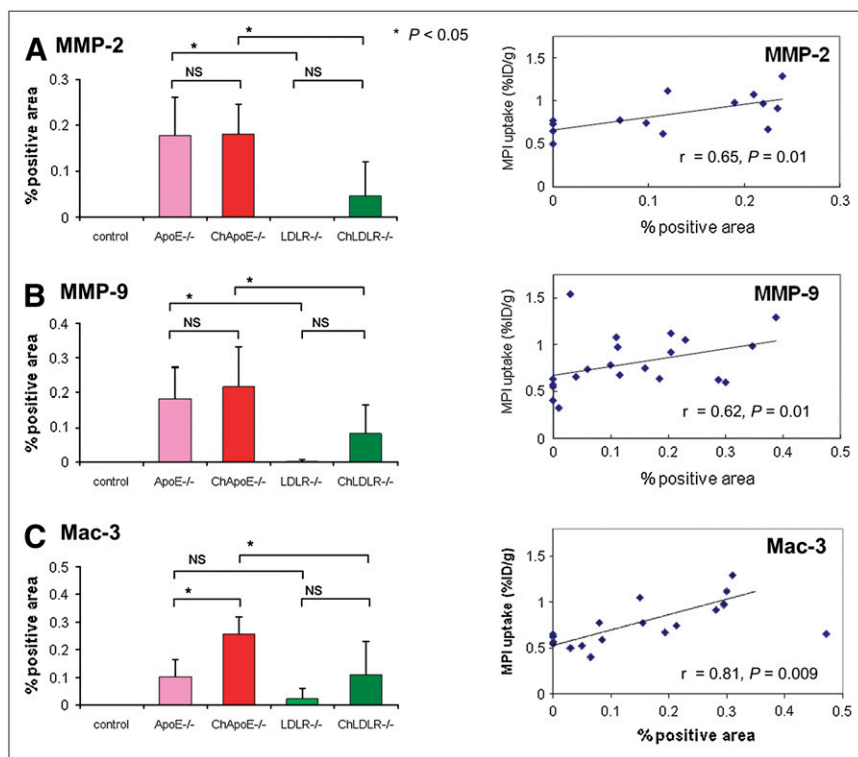
The present study demonstrated the feasibility of noninvasive detection of MMP activity in atherosclerotic lesions, using a radiolabeled broad-spectrum inhibitor of active MMPs. The extent of pathologic lesions, plaque infiltration, and MPI uptake was highest in the most advanced lesions and strongly correlated with the extent of plaque infiltration and quantitative expression of MMP-2 and MMP-9. Because MMP expression is higher in unstable than in stable coronary lesions, MPI imaging could be used to detect high-risk, unstable lesions. It is recognized that specific metalloproteinases contribute to atherosclerotic lesions differently and may play an important role in different stages of plaque evolution. It is therefore possible that radiotracers targeted at specific metalloproteinases may be more informative prognostically.

Unstable atherosclerotic plaques obtained from patients dying of acute coronary events often reveal intense inflammation. The monocyte-macrophage infiltration in atherosclerotic plaque is accompanied by production of inflammatory cyto-

kines such as tumor necrosis factor- α , interleukin-1 (15–17), and MMP (18). Elevated MMP messenger RNA, protein, and MMP activity have been reported in the fibrous cap and necrotic cores of the atherosclerotic plaques (19,20). It has been proposed that increased MMP activity contributes to fibrous cap attenuation (19,21) and expansive outward vascular remodeling (21,22).

In ApoE^{-/-} receiving a high-cholesterol diet, the gene expression of MMP-9 increases with age and progression of atherosclerotic lesions and is accompanied by an increase in other proteases, such as cystatin-C and cathepsins (23). Positive vascular remodeling in ApoE^{-/-} after carotid ligation is associated with increased accumulation of neo-intimal foam cell macrophages and increased expression of MMP-2 and MMP-9 (24,25). Similarly, increased expression of MMP-3, MMP-12, and MMP-13 has been reported not only in atherosclerotic lesions but also in aneurysms in LDLR^{-/-} (26). In ApoE^{-/-}, overexpression of MMP-9 in macrophages has been observed in advanced atherosclerotic lesions and is commonly associated with plaque rupture (27) and intraplaque hemorrhage (28). Conversely, in ApoE^{-/-}, MMP-9 deficiency is reported to be associated with reduced atherosclerosis, medial layer attenuation (29), and vascular remodeling (30). Similar observations have been reported in the MMP-2/ApoE double-knockout mice (31). In ApoE^{-/-} demonstrating MMP-12 deficiency, reduced atherosclerosis is associated with a lower likelihood of aneurysmal dilation of the aorta (29), and MMP-13 deletion promotes collagen accumulation and plaque stabilization (32). In contrast, ApoE^{-/-} with overexpression of MMP-1 have less atherosclerosis (33), and MMP-3-inactivated ApoE knockout mice

FIGURE 4. Quantitative histologic analysis of MMP-2 (A), MMP-9 (B), and macrophage (C) expressions in aortic tissue specimens from the 5 study groups and their correlation with %ID/g uptake. Percent positive areas are presented as mean \pm SD in each group. When 1 outlier observation from immunohistochemical staining for macrophages was removed (C), correlation between %ID/g uptake became highly significant. Ch = high-cholesterol-fed.



have less advanced atherosclerosis (34). In these transgenic models, each MMP also plays a different role in the different stages of atherosclerotic disease (25,35). Although plaque rupture is not unusual in transgenic atherosclerotic animal models, targeting of MMP activity in plaques offers a proof of principle that molecular imaging could become clinically useful in the identification of plaque vulnerability.

CONCLUSION

This study demonstrated that molecular imaging with radiolabeled MMP inhibitor allows detection of MMP activity in a wide spectrum of atherosclerotic lesion severities in transgenic mouse models. Because MMP activity directly correlates with plaque vulnerability, noninvasive assessment of MMP activity is expected to allow identification of unstable plaques.

ACKNOWLEDGMENTS

This study was supported by National Institutes of Health grant RO1 (HL 078681) to Dr. Narula and, in part, by a grant-in-aid from Fukuda Foundation for Medical Technology. The radiolabeled imaging agent was provided by Lantheus Medical Imaging.

REFERENCES

- Libby P. Inflammation in atherosclerosis. *Nature*. 2002;420:868–874.
- Libby P, Ridker PM, Maseri A. Inflammation and atherosclerosis. *Circulation*. 2002;105:1135–1143.
- Hartung D, Sarai M, Petrov A, et al. Resolution of apoptosis in atherosclerotic plaque by dietary modification and statin therapy. *J Nucl Med*. 2005;46:2051–2056.
- Hartung D, Schafers M, Fujimoto S, et al. Targeting of matrix metalloproteinase activation for noninvasive detection of vulnerable atherosclerotic lesions. *Eur J Nucl Med Mol Imaging*. 2007;34(suppl 1):s1–s8.
- Fujimoto S, Hartung D, Edward DS, et al. Molecular imaging of matrix metalloproteinase in atherosclerotic lesions: resolution with dietary modification and statin therapy. *J Am Coll Cardiol*. 2008;52:1847–1857.
- Deguchi JO, Aikawa M, Tung CH, et al. Inflammation in atherosclerosis: visualizing matrix metalloproteinase action in macrophages in vivo. *Circulation*. 2006;114:55–62.
- Schafers M, Riemann B, Kopka K, et al. Scintigraphic imaging of matrix metalloproteinase activity in the arterial wall in vivo. *Circulation*. 2004;109:2554–2559.
- Su H, Spinale FG, Dobrucki LW, et al. Noninvasive targeted imaging of matrix metalloproteinase activation in a murine model of postinfarction remodeling. *Circulation*. 2005;112:3157–3167.
- Johnson JL, Jackson CL. Atherosclerotic plaque rupture in the apolipoprotein E knockout mouse. *Atherosclerosis*. 2001;154:399–406.
- Ishibashi S, Herz J, Maeda N, Goldstein JL, Brown MS. The two-receptor model of lipoprotein clearance: tests of the hypothesis in “knockout” mice lacking the low density lipoprotein receptor, apolipoprotein E, or both proteins. *Proc Natl Acad Sci USA*. 1994;91:4431–4435.
- Nakashima Y, Plump AS, Raines EW, Breslow JL, Ross R. ApoE-deficient mice develop lesions of all phases of atherosclerosis throughout the arterial tree. *Arterioscler Thromb*. 1994;14:133–140.
- Calara F, Silvestre M, Casanada F, Yuan N, Napoli C, Palinski W. Spontaneous plaque rupture and secondary thrombosis in apolipoprotein E-deficient and LDL receptor-deficient mice. *J Pathol*. 2001;195:257–263.
- Jackson CL, Bennett MR, Biessen EA, Johnson JL, Krams R. Assessment of unstable atherosclerosis in mice. *Arterioscler Thromb Vasc Biol*. 2007;27:714–720.

- Stary HC, Chandler AB, Dinsmore RE, et al. A definition of advanced types of atherosclerotic lesions and a histological classification of atherosclerosis: a report from the Committee on Vascular Lesions of the Council on Arteriosclerosis, American Heart Association. *Arterioscler Thromb Vasc Biol*. 1995;15:1512–1531.
- Kolodgie FD, Virmani R, Burke AP, et al. Pathologic assessment of the vulnerable human coronary plaque. *Heart*. 2004;90:1385–1391.
- Virmani R, Burke AP, Farb A, Kolodgie FD. Pathology of the vulnerable plaque. *J Am Coll Cardiol*. 2006;47(8, suppl):C13–C18.
- Virmani R, Kolodgie FD, Burke AP, Farb A, Schwartz SM. Lessons from sudden coronary death: a comprehensive morphological classification scheme for atherosclerotic lesions. *Arterioscler Thromb Vasc Biol*. 2000;20:1262–1275.
- Galis ZS, Sukhova GK, Krantzhofer R, Clark S, Libby P. Macrophage foam cells from experimental atheroma constitutively produce matrix-degrading proteinases. *Proc Natl Acad Sci USA*. 1995;92:402–406.
- Sukhova GK, Schonbeck U, Rabkin E, et al. Evidence for increased collagenolysis by interstitial collagenases-1 and -3 in vulnerable human atheromatous plaques. *Circulation*. 1999;99:2503–2509.
- Herman MP, Sukhova GK, Libby P, et al. Expression of neutrophil collagenase (matrix metalloproteinase-8) in human atheroma: a novel collagenolytic pathway suggested by transcriptional profiling. *Circulation*. 2001;104:1899–1904.
- Galis ZS, Sukhova GK, Lark MW, Libby P. Increased expression of matrix metalloproteinases and matrix degrading activity in vulnerable regions of human atherosclerotic plaques. *J Clin Invest*. 1994;94:2493–2503.
- Brown DL, Hibbs MS, Kearney M, Loushin C, Isner JM. Identification of 92-kD gelatinase in human coronary atherosclerotic lesions: association of active enzyme synthesis with unstable angina. *Circulation*. 1995;91:2125–2131.
- Jormsjo S, Wuttge DM, Sirsjo A, et al. Differential expression of cysteine and aspartic proteases during progression of atherosclerosis in apolipoprotein E-deficient mice. *Am J Pathol*. 2002;161:939–945.
- Ivan E, Khatri JJ, Johnson C, et al. Expansive arterial remodeling is associated with increased neointimal macrophage foam cell content: the murine model of macrophage-rich carotid artery lesions. *Circulation*. 2002;105:2686–2691.
- Newby AC. Dual role of matrix metalloproteinases (matrixins) in intimal thickening and atherosclerotic plaque rupture. *Physiol Rev*. 2005;85:1–31.
- Prescott MF, Sawyer WK, Von Linden-Reed J, et al. Effect of matrix metalloproteinase inhibition on progression of atherosclerosis and aneurysm in LDL receptor-deficient mice overexpressing MMP-3, MMP-12, and MMP-13 and on restenosis in rats after balloon injury. *Ann N Y Acad Sci*. 1999;878:179–190.
- Gough PJ, Gomez IG, Wille PT, Raines EW. Macrophage expression of active MMP-9 induces acute plaque disruption in apoE-deficient mice. *J Clin Invest*. 2006;116:59–69.
- de Nooijer R, Verkleij CJ, von der Thusen JH, et al. Lesional overexpression of matrix metalloproteinase-9 promotes intraplaque hemorrhage in advanced lesions but not at earlier stages of atherogenesis. *Arterioscler Thromb Vasc Biol*. 2006;26:340–346.
- Luttun A, Lutgens E, Manderveld A, et al. Loss of matrix metalloproteinase-9 or matrix metalloproteinase-12 protects apolipoprotein E-deficient mice against atherosclerotic media destruction but differentially affects plaque growth. *Circulation*. 2004;109:1408–1414.
- Lessner SM, Martinson DE, Galis ZS. Compensatory vascular remodeling during atherosclerotic lesion growth depends on matrix metalloproteinase-9 activity. *Arterioscler Thromb Vasc Biol*. 2004;24:2123–2129.
- Kuzuya M, Nakamura K, Sasaki T, Cheng XW, Itohara S, Iguchi A. Effect of MMP-2 deficiency on atherosclerotic lesion formation in apoE-deficient mice. *Arterioscler Thromb Vasc Biol*. 2006;26:1120–1125.
- Deguchi JO, Aikawa E, Libby P, et al. Matrix metalloproteinase-13/collagenase-3 deletion promotes collagen accumulation and organization in mouse atherosclerotic plaques. *Circulation*. 2005;112:2708–2715.
- Lemaitre V, O’Byrne TK, Borczuk AC, Okada Y, Tall AR, D’Armiento J. ApoE knockout mice expressing human matrix metalloproteinase-1 in macrophages have less advanced atherosclerosis. *J Clin Invest*. 2001;107:1227–1234.
- Silence J, Lupu F, Collen D, Lijnen HR. Persistence of atherosclerotic plaque but reduced aneurysm formation in mice with stromelysin-1 (MMP-3) gene inactivation. *Arterioscler Thromb Vasc Biol*. 2001;21:1440–1445.
- Janssens S, Lijnen HR. What has been learned about the cardiovascular effects of matrix metalloproteinases from mouse models? *Cardiovasc Res*. 2006;69:585–594.